Surface charge of acidic sophorolipids micelles: effect of base and time

Authors

Niki Baccile,[a,b,c]* Jan Skov Pedersen,[d] Gerard Pehau-Arnaudet,[e] Inge Van Bogaert[f]

Affiliations

a -UPMC Univ Paris 06, UMR 7574, Chimie de la Matière Condensée de Paris, F-75005, Paris, France. E-mail : niki.baccile@upmc.fr

b - CNRS, UMR 7574, Chimie de la Matière Condensée de Paris, F-75005, Paris, France

c – Collège de France, UMR 7574, Chimie de la Matière Condensée de Paris, F-75005, Paris, France

d - Department of Chemistry and iNANO Interdisciplinary Nanoscience Center, Aarhus University, DK-8000 Aarhus, Denmark

e. Plate-Forme de Cryomicroscopie Moléculaire, URA 2185, Institut Pasteur, 28 Rue du Docteur Roux, F-75015, Paris, France

f. InBio, Department of Biochemical and Microbial Technology, Faculty of Bioscience Engineering, Ghent University, Coupure Links 653, 9000, Ghent, Belgium

Abstract

Acidic sophorolipids, SL-COOH, bio-derived glycolipids, are known to form micelles whose interactions vary as a function of pH. Upon partial ionization of the COOH group, intermicellar interactions take place. Here, we explore the nature of these interactions by using Small Angle Neutron Scattering (SANS) on SL-COOH solutions to which increasing amounts of NaOH are added. The effect of the nature of the base is also explored by replacing NaOH with aqueous NH_3, KOH and $Ca(OH)_2$. Time effects up to 36 days are also discussed. All SANS data have been successfully fitted using an appropriate model of core-shell ellipsoids of revolution with an interaction potential, U(r), which combines hard-sphere and screened Coulomb (described by a repulsive Yukawa potential) potentials. Modelling quantifies the effect of the base in terms of micellar size, effective surface charge and interfacial hydration thus showing the possibility to tune them at will.

Introduction

The emerging field of biosurfactants has been intensively studied in the past 20 years to address the expectations of replacing non-renewable, petro-derived, compounds.[1] Glycolipids, in particular, are surface active agents composed of a carbohydrate-based hydrophilic head covalently linked to a fatty acid or a fatty alcohol.[2] The enhanced biodegradability of these products has made them interesting candidates to replace common surface active agents in the formulation of home and personal care products. For these reasons, they have been intensively studied in the past 15 years.[2,3,4] In this field, entirely bio-derived glycolipids, like rhamnolipides or sophorolipids, have a specific interest for several reasons. These compounds are entirely bio-sourced, that is, they are derived in fairly large amounts from yeasts or bacteria, grown in presence of glucose and fatty acids but even alkanes and waxes.[5-8] Due to their reduced environmental impact,[9] sophorolipids (SL) have particularly attracted a fair attention for applications in home and skin-care products[10-,11,12] but also for their anticancer, antimicrobial and self-assembly properties. [8,13,14]

The raw form of SL is actually a mixture of the lactone and acidic form and whose percentage in the culture medium is never constant. For this reason, a specific treatment is requested to isolate either one form or the other. Acidic sophorolipids, SL-COOH (Figure 1), are particularly interesting as they are composed of a sophorose unit attached to an oleic acid moiety through an ether bond on the C17 carbon atom of the fatty acid chain. This particular feature leaves the COOH group unaffected, making this compound sensitive to pH, where stimuli-responsive (temperature, electric field, ionic strength and pH, solvent) properties are extremely important for the development of a number of applications in many different fields: stabilization of emulsions, suspensions or foams, drug encapsulation and delivery, wettability control, enhancement of viscoelastic properties, recyclability, heat-transfer fluids, drag-reduction agents, dynamic templating for nanomaterials, smart hydrogels for wound healing, artificial muscle conception.

The self-assembly and stimuli-responsive properties of sophorolipids have been scarcely studied in the past few years and recent works show the interesting features of this compound in response to pH. Supramolecular assembling dependence is known since 2004[8] but more detailed pieces of information have been achieved since 2010.[14,15,16,17] In our early work,[14] we have mainly shown how SL-COOH based micelles can be exploited as porogenic agents for the synthesis of silica thin films. SANS data show how pH strongly affects the long-range interactions among SL-COOH micelles. Th pH-responsive behaviour has been addressed in a specific work[15] in which we put in evidence three distinct regimes during

which the self-assembly of SL-COOH is different. In Regime 1 at acidic pH, individual micelles exist in solution. Upon increase of the pH, the system goes to regime 2, where the increasing amount of COO^- groups introduces repulsive interactions between micelles, as evidenced by the appearance of an interaction peak in SANS spectra. Finally, regime 3 identifies the critical point at which most micelles are disrupted in favour of larger interconnected tubular objects, much bigger in size. Penfold and co-workers[16] also propose the presence of globular micelles, small vesicles and tubules on several types of sophorolipids in their lactonic and acidic, both diacetylated and non-acetylated, forms.

In this paper, we explore further the effect of base addition (NaOH) and type of base (KOH, NH_3, $Ca(OH)_2$) on micellar assembly in what we previously addressed to as region 2, where intermicellar interactions dominate the SANS spectra, which include significant influence of the structure factor, S(q), component of the diffused intensity. The presence of S(q) makes the quantitative analysis and interpretation of the spectra difficult without using a specific model to analyze the data and which we propose and discuss here to fit SANS spectra. Additionally, using the same model, we also address the issue of time effects on SL-COOH self-assembly, which was proposed several years ago[8] and never studied again. In fact, even if the formation of micrometer-sized filaments with time was previously shown, nothing is actually known on the local micellar environment in the previously described pH-dependant regimes.

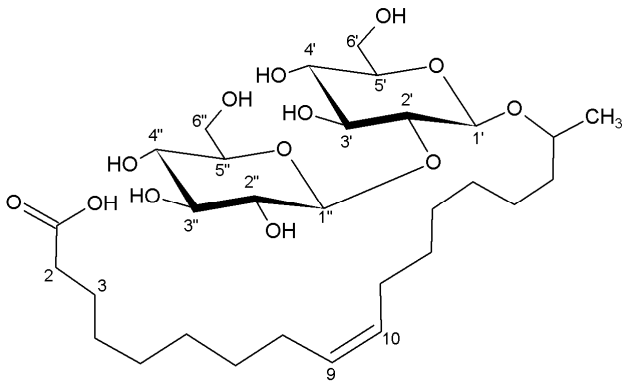

Figure 1 – Acidic form of sophorolipids (SL) obtained from *Candida bombicola*

Experimental

Sample preparation. The synthesis of acidic sophorolipids (SL-COOH) was described previously.[15] For the pH and cation effects, we focused on the regime 2 sample preparation.[15] Typically, concentration is 50 mg/mL in D_2O to which μmolar amounts (the

end molar concentration is given on each figure) of NaOH, KOH, aqueous NH_3 and $Ca(OH)_2$ solutions have been added. All samples are analyzed within 24 hours from their preparation. Time-dependency has been mainly tested for regime 2 ([NaOH]= 58 mM) but regime 1 and 3[15] are also explored in terms of comparison. Typical storing for these experiments are: T= 22°C under static conditions during 8, 14, 21 and 36 days. To reduce evaporation effects, 2 mL Eppendorf tubes are filled as much as possible (about 1.8 mL of the sophorolipid solution).

Experimental techniques. Transmission Electron Microscopy under cryogenic conditions (Cryo-TEM) was run on a Jeol 2010F at the PFMU, Institut Pasteur (Paris, France). The microscope operates at 200 kV and magnification was 80.000 fold. A Gatan ultrascan 4000 camera was used to acquire the images. DigitalMicrograph™ software was used. Cryofixation was done on a EMGP, Leica (Austria) instrument. Liquid samples at desired concentrations were deposited on TEM copper grids coated with a carbon layer containing holes of 2 μm (Quantifoil R2/2, Quantifoil, Germany). Excess of sample was blotted and the grid was immediately frozen into liquid ethane. All grids were stored and processed at liquid nitrogen throughout all experimentation. Samples were transferred to the microscope using a Gatan Cryoholder (Gatan 626DH, Gatan, USA).

Small Angle Neutron Scattering (SANS) was performed at the Léon Brillouin Laboratory (LLB, Orphée Reactor, Gif-sur-Yvette, France) on the PACE beamline. The spectrometer configuration was adjusted to cover two different *q*-ranges. The small angle region $6.90 \cdot 10^{-3}$ $Å^{-1} < q < 7.30 \cdot 10^{-2}$ $Å^{-1}$ is obtained with a neutron wavelength, λ, of 6 Å and a sample-to-detector distance, D, of 4.7 m. An acquisition time of 3960 s was used; the medium angle region covers a q-range $2.90 \cdot 10^{-2}$ $Å^{-1} < q < 3.00 \cdot 10^{-1}$ $Å^{-1}$ at λ= 6 Å with D= 1.0 m. An acquisition time of 1770 s was used in that case. q is defined as $(4\pi/\lambda)\sin\theta/2$, where θ is the scattering angle between the incident and the scattered neutron beams. All samples are introduced in a 2 mm quartz cell and studied at T= 22°C. The blank sample is composed of 99.9% D_2O, whose signal is subtracted from the experimental data. Data treatment is done with the PAsiNET.MAT software package provided at the beamline and available free of charge.[18] Absolute values of the scattering intensity are obtained from the direct determination of the number of neutrons in the incident beam and the detector cell solid angle. The 2D raw data were corrected for the ambient background and empty cell scattering and normalized to yield an absolute scale (cross section per unit volume) by the neutron flux on the samples. The

data were then circularly averaged to yield the 1-D intensity distribution, I(q). I(q) spectra are presented in this work in a lin-log scale to show at best intensity variations.

Fit of SANS data.

The intensity is modeled by the following expression:

$$I(q) = n(\rho_{core} - \rho_0)^2 P(q) S(q) = n(\rho_{shell} - \rho_0)^2 \left(\frac{P(q)}{\alpha^2}\right) S(q) \qquad \text{Eq 1}$$

where $n = \frac{N}{V_{tot}}$ is the number density of the scatterers used for normalizing the intensity per unit volume. $S(q)$ is the structure factor while $P(q)$ is the form factor of the micelles. For this study, we considered either a spherical or an ellipsoidal form factor and both are described using a core/shell model. α is a core/shell contrast term, $\alpha=(\rho_{shell}-\rho_0)/(\rho_{core}-\rho_0)$, with ρ_0, ρ_{shell} and ρ_{core} being the scattering length densities (SLD) of, respectively, the solvent, the hydrophilic shell and the hydrophobic core. Form factors for core-shell spheres and ellipsoids are well-known and can be found, for instance, in Ref.19. Here, the globular micelles are described using a core radius R_c, an external corona of width R_h, a total radius R_c+R_h, an eccentricity L/R_c of the core and a polydispersity σ of the radii, as shown in Figure 2.

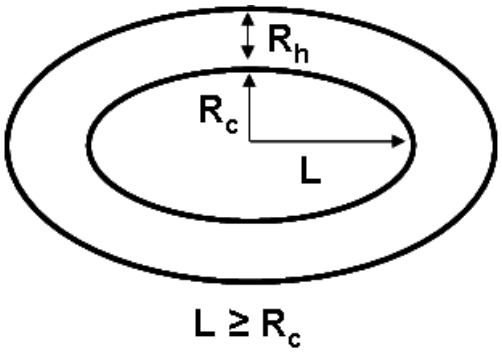

Figure 2 – Globular core-shell micelle model used to calculate the form factor. R_h is the corona width, R_c is the core radius and L is the major axis length. For an ellipsoid, L> R_c and for a sphere, L=R_c.

The interaction potential, U(r), used in this study combines hard-sphere and screened Coulomb (described by a repulsive Yukawa potential) potentials and reads:

$$U(r) = +\infty \quad r < D_{HS} \qquad \text{Eq 2}$$

$$U(r) = U_0 \frac{D_{HS}}{r} \exp(-\kappa(r - D_{HS})) \quad r > D_{HS}\ , \qquad \text{Eq 3}$$

where, for convenience, in the *U(r)* expression the sign has been omitted. In fact, r is the minimum distance between two micelles, $D_{HS} = 2R_{HS}$ the hard-sphere interaction diameter,

and U_0 (in k_BT unit) the strength of the potential at r= D_{HS}, where for $U_0 > 0$, the potential is repulsive while for $U_0 < 0$, the potential is attractive. κ stands for the range (inverse of the Debye length, λ) of the potential. The potential strength can be related to the charge of the system according to

$$\left|U_0\right| = \frac{Q^2}{\varepsilon_o \varepsilon_r D_{HS}(2 + \kappa D_{HS})} \qquad \text{Eq 4}$$

with Q being the particle charge (Q= Ze, the micellar valence and the electron charge) and ε_0, ε_r are the vacuum permittivity and the solvent relative permittivity, respectively. The expression for κ in the case of a single ion of concentration *c* and charge *q* for an ideal solution as predicted by the Gouy-Chapman Debye-Huckel Poisson-Boltzmann theory is

$$\kappa = \frac{1}{\lambda} = \left(\frac{4\pi c q^2}{\varepsilon_o \varepsilon_r k_b T}\right)^{1/2} \qquad \text{Eq 5}$$

where k_b is the Boltzmann constant and T the absolute temperature.

We use here an analytical expression of the structure factor *S(q)* for the interaction potential $U(r)$, that is obtained in the Mean Spherical Approximation (MSA)[20], assuming that the Yukawa potential is a weak repulsive tail:

$$S_{Yukawa}(q) = \frac{1}{1 + n c_{HS}(q) + n c_{Yukawa}(q)} \qquad \text{Eq 6}$$

where *n* has been defined before as the number of micelles per unit volume. The term $c_{HS}(q)$ is the direct correlation function for a simple hard-sphere interaction, where the hard-sphere volume fraction is ϕ_{HS}

$$nc_{HS}(q) = 24\phi_{HS} A(qD_{HS}) / (qD_{HS})^6 \qquad \text{Eq 7}$$

with

$$A(x) = 24\gamma_{HS} - 2\beta_{HS}x^2 - \cos(x)\left(24\gamma_{HS} - 2(\beta_{HS} + 6\gamma_{HS})x^2 + (\alpha_{HS} + \beta_{HS} + \gamma_{HS})x^4\right) + x\sin(x)\left(-24\gamma_{HS} + (\alpha_{HS} + 2\beta_{HS} + 4\gamma_{HS})x^2\right) \qquad \text{Eq 8}$$

$$\alpha_{HS} = \frac{(1 + 2\phi_{HS})^2}{(1 - \phi_{HS})^4} \quad \beta_{HS} = -\phi_{HS}\frac{3}{2}\frac{(2 + \phi_{HS})^2}{(1 - \phi_{HS})^4} \quad \gamma_{HS} = \frac{\alpha_{HS}\phi_{HS}}{2} \qquad \text{Eq 9}$$

and :

$$nc_{Yukawa}(q) = -24\frac{\phi_{HS}U_0}{D_{HS}^2 q\left(\kappa^2 + q^2\right)}\left(q\cos(qD_{HS}) + \kappa\sin(qD_{HS})\right) \qquad \text{Eq 10}$$

Finally, the low-q portion ($q< 0.01$ Å^{-1}) of the spectra has been fitted by adding a power-law term, $q^{-\beta}$, where $1 < \beta < 2$, to the expression of I(q). All data have been treated using a least-square fitting procedure.[21]

Results and discussion

The fitting model. As it was proposed before,[16] and considering the molecular structure of sophorolipids, it is reasonable to use a core-shell model: the sophorose group identifies the hydrophilic shell while the oleic acid moiety is associated with the hydrophobic core. R_h and R_c refer, respectively, to the shell and core sizes, whereas (R_c+R_h) represents the overall cross-micellar radius. For the specific case of lactonic sophorolipids, Penfold et al.[16] also proposed a vesicle shape with a double surfactant layer and an inner water-rich core. This choice is in agreement with the molecular structure of sophorolipids and it raises important, unsolved, questions even for the acidic form of the compound. In fact, tentatives to describe the local conformation of the oleic acid chain and the exact positioning of the COOH group have been done for acidic sophorolipids[15] and similar bolaform systems,[22] but a clear answer is not yet found.

In terms of the type of shape, three simple forms can be employed: sphere, ellipsoid and cylinder. The choice is relatively easy when no intermicellar interactions are present, that is for unitary values of the structure factor, S(q), which occur in the regime 1 for the SL-COOH system. In regime 2, where $S(q) \neq 1$, spherical/elliptical objects are rather observed. For this reason, we tested a sphere and ellipsoid of revolution form factors to fit SANS spectra presented here. In particular, as argumented in the following, the two-axis core-shell ellipsoid of revolution (R_c= inner core cross-radius; R_h= width of the corona; L= ellipsoid half length; Figure 2) is actually preferred over the sphere.

Beyond the shape, the model also takes into account the core (ρ_{core}), shell (ρ_{shell}) and solvent densities (ρ_0), which are summarized in the α parameter, $\alpha = (\rho_{shell}-\rho_0)/(\rho_{core}-\rho_0)$. Experiments have been run in D_2O, for which the neutron Scattering Length Density (SLD) is known to be $\rho_0 = 6.36 \cdot 10^{-6}$ Å^{-2}. Estimating the SLD for sophorolipids in water, and in particular the core and shell components is more delicate. To do so, we used the NIST database calculator[23] in which we separately calculated the sophorose ($C_{12}H_{21}O_{10}$) and oleic acid ($C_{18}H_{35}O_3$) contributions, nevertheless taking the sophorolipids density (1.097 g·cm^{-3}). The theoretical α value from the known SLD of D_2O (ρ_0), core (ρ_{core}) and shell (ρ_{shell}) for sophorolipids is 0.83 and a preliminary set of fits was done (results not shown) keeping this

parameter constant. Then, α was set as a free variable. In this case, the fit was controlled by assuming that the effective micellar shell density (ρ_{shell}) should always be contained between the solvent (ρ_0) and the theoretical SLD of the sophorose layer, $\rho_{shell}(sophorose)= 1.20 \cdot 10^{-6}$ Å^{-2}. Finally, the structure factor is characterized by four parameters: the volume fraction, ϕ, the hard-sphere radius, R_{HS}, the potential strength (in K_bT units), U_0/K_bT and the screening parameter, κ (refer to Eq.2-5, Eq.7 and Eq.10). The most important parameters in the fit, their value and units are summarized in Table 1.

Table 1

Parameter	**Description**	**Value in the fit**
R_c	Core radius (Å)	Variable
R_h	Corona size/width (Å)	Variable
L	Ellipsoid longer dimension (Å). For a sphere, L= R_c	Variable
α	Contrast term (dimensionless)	Variable
ϕ	Volume fraction (dimensionless)	0.05
U_0/K_bT	Potential strength (in K_bT scale, dimensionless)	Variable
κ	Screening parameter (1/Å)	Fixed, calculated according to Eq.5
R_{HS}	Hard sphere radius (Å)	Variable
σ	Radius polydispersity	0.01
I_0	Scaled intensity factor	Variable

The volume fraction, ϕ, is fixed to 0.05, a value which is related to the initial SL-COOH concentration (50 mg/mL). In terms of the form factor, its choice is always difficult in the presence of intermicellar interactions. Here, we decided to use an ellipsoid with low polydispersity on its radius (σ= 0.01, fixed parameter) rather than a sphere. In fact, the lack of typical spectral oscillations expected at high-q for monodisperse spheres requires the use of large polydispersity values (> 0.3), as already described before.[15] In this case, one may always wonder which is the origin of polydispersity in fitting a spherical system: dispersion in size or in shape? Other arguments justify the use of an ellipsoid form factor. If a spherical form factor

is used, the average ρ_{shell} (α set as a variable parameter) from the fit at different NaOH concentrations is ρ_{shell}~ $5.81 \cdot 10^{-6}$ Å^{-2}, which is less than 10 % smaller than the value calculated for ρ_0. This corresponds to a hydration level of the sophorose shell of more than 99 %. On the contrary, the ellipsoidal model provides $3.40 < \rho_{shell}$ [$\cdot 10^{-6}$ Å^{-2}] < 4.80. This range of values indicates a more contained (between 91 % and 96 %), though still high, hydration degree of the sophorose, which we reasonably prefer for further analysis. Finally, the use of a sphere form factor has an impact of on the evolution of the micellar typical radius, which would be above 30 Å. This value is in contrast with our previous cryo-TEM observations that showed an average size of about 22 Å.[15]

The choice of a variable α parameter on the fit is now discussed. In principle, this parameter can be fixed to a theoretical value of 0.83. In practice, this is very restrictive and we verified that a variable α hasn't any significant impact neither on the quality nor on the trend of the main fit parameters (e.g., radii, eccentricity, potential strength). Tests (not presented here) show that the most important discrepancies concern the absolute values of R_c and L/R_c, respectively over- and under-estimated (5-10 %) for the variable-α configuration of the fit. In terms of their trend as a function of increasing NaOH concentration, both R_c and L/R_c decrease. For the rest of the fits, at least two arguments justify the choice of keeping α as a variable: 1) fixing α means to define a clear-cut interface between water and sophorose, which is not consistent with the strong hydrophilic nature of this group in non-acetylated SL-COOH.[16,17] This is also not consistent with the increasing negative charge of the micellar interface, as demonstrated in this work. 2) At fixed α, the fit always converges for an average size of the micellar core of about 9 Å; the fully extended (calculated) oleic acid chain (C_{18}) is not less than 26 Å[24] and, even in case of bending, this value can hardly be lower than 12-14 Å, where possible bending of the C_{18} chain has been proposed both by us[15] and Penfold.[16] These considerations suggest that keeping α= 0.83 does not provide a consistent value for the actual chain size.

Finally, in order to simplify the fitting procedure and reduce the number of free variables, the screening parameter, κ, is calculated according to Eq.5 and kept constant throughout the fit. Nevertheless, one should be aware that the Debye length ($1/\kappa$) can be affected by the nature of the micellar counter-ion. This is specifically discussed in the text.

NaOH addition. Given the molecular formula of SL-COOH, addition of a base enhance the amount of carboxylates, which presumably surround the sophorolipid micelle and introduce

repulsive intermicellar interactions. This assumption is studied here in Figure 3 by observing SANS data of SL-COOH under slightly different NaOH concentrations. Increasing the amount of base from 10.3 mM to 66.7 mM provokes the appearance of an interaction peak in the mid-q region below q= 0.1 $Å^{-1}$. These data are also characterized by a steep increase of the SANS intensity at q< 0.015 $Å^{-1}$, whose slope in a log-log scale is contained between -1 and -2. The fits of these spectra using a core-shell ellipsoidal form factor in presence of Yukawa-type electrostatic potential are shown as solid lines in Figure 3. This model allows a very good fit for the whole SANS data set. A more quantitative analysis is presented in the evolution of fit parameters in Figure 4a-d.

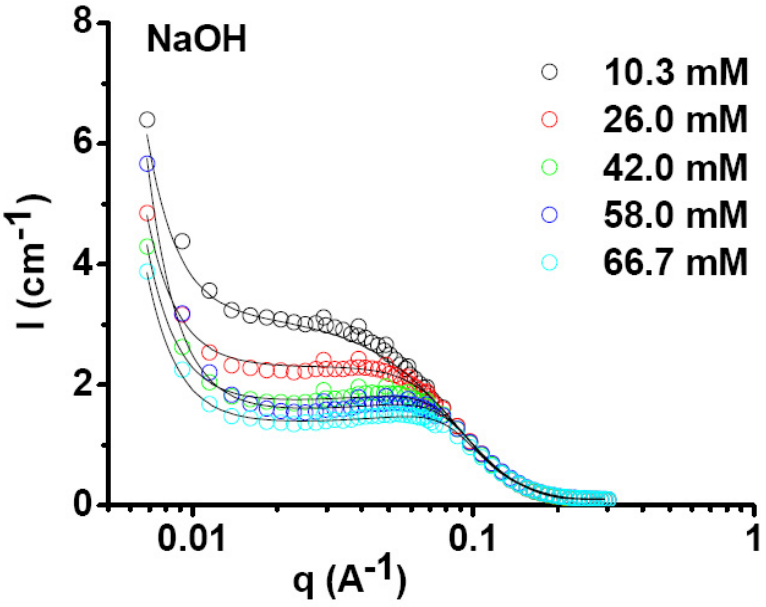

Figure 3 – SANS spectra recorded on a SL-COOH system at different (final) concentrations of NaOH, given in the legend. Solid lines represent the fits obtained using an ellipsoid of revolution form factor and variable α-paramter. One can refer to the main text for more information on the model.

The choice of a structure factor related to the Yukawa potential is justified by the supposed electrical charge variations of the micelles upon incrementing pH (formation of COO- groups from SL-COOH). In fact, a typical hard-sphere potential is not suited for this system as the S(q) term would only depend on R_{HS} and the volume fraction, ϕ, which is actually constant. In Figure 4a we show the evolution of the potential strength, U_0/K_bT, defined in Eq.3 with the amount of NaOH. First of all, the sign of U_0/K_bT obtained in the fit is positive, indicating an overall positive value of the Yukawa potential. According to the sign convention chosen to describe the potential on Eq.3, the interactions between micelles are clearly repulsive. Secondly, the absolute value of U_0/K_bT increases with the amount of NaOH. Since U_0/K_bT is proportional to the effective micellar charge (Eq.4), the evolution of this

parameter shown in Figure 4a indicates that the micelles become more and more negatively charged upon addition of NaOH. The effective charge, Z, can be estimated from Eq.4 itself (using the equivalence Q= Ze) and it varies from about 0.5 to 5.3 when NaOH goes from 10.3 mM to 66.7 mM. The repulsive interactions also affect the hard sphere radius, R_{HS}, which decreases from 35.4 Å to 26.4 Å, which is expected for strongly interacting micelles and in agreement to the trend of the (calculated) Debye length, λ, (Eq.5), plotted in Figure 4a, which also decreases from 16.1 Å to 6.3 Å due to the higher Na^+ concentration in solution.

In terms of micellar size, Figure 4b reports the total effective cross-radius of the micelle, R_c+R_h and it seems to decrease from 21.8 Å to 18.2 Å with increasing NaOH; in particular, the main contribution to this effect seems to come from R_c alone, which decreases from 14.2 Å to 10.9 Å, the size of the sophorose shell, R_h, being practically constant (~ 8 Å). According to the model, the micellar core corresponds to the oleic acid moiety; its typical size deduced from the fit is always below 15 Å. As commented in previous works,[15,16] one expects the size of the oleic acid chains to be well above 20 Å in an ideal fully elongated configuration but this does not seem to be the case, bringing some support to the idea of a parallel SL-COOH configuration followed by folding of the chain. An additional remark concerns R_c, which decreases with increasing $[OH^-]$. This can be explained by the fact that the formation of larger amounts of COO^-/Na^+ ion pairs consequently induce increasing amount of oleic acid moieties to bend outward, towards the micelle/solvent palisade.

In terms of the micellar shape evolution, increasing $[OH^-]$ seems to slightly affect the micellar eccentricity, which goes from 3.3 to 2.6, indicating a tendency to form more spherical micelles. First of all, having more elongated micelles at low amount of NaOH is coherent with our previous data recorded in a NaOH-free medium, where SL-COOH micelles are described by small cylinders. When the effective micellar surface charge increase (increasing U_0/K_bT, Figure 4a), one can expect local repulsion between close sophorolipid molecules. This effect can contribute to decrease the micellar eccentricity and, consequently, to increase the micellar curvature. Finally, it is very interesting to follow the hydration level of the sophorose head, as shown in Figure 4d. For low amounts of NaOH, the resulting SLD is close to $5 \cdot 10^{-6}$ $Å^{-2}$, a value which indicates that the micellar shell is actually composed of not much less than 96% of water. Addition of the base induces a significant reduction of ρ_{shell} ($3.40 \cdot 10^{-6}$ $Å^{-2}$ at 66.7 mM) which translates into an additional 5% loss in interface water. This trend showing a loss of shell water can probably be related to the bending of the oleic acid chain and the presence of the sodium carboxylate ion pair. One could actually wonder if the contribution of COO^-Na^+ has any effect on the theoretical SLD of the sophorose shell. If that would be included in the

calculation, the effective SLD value of sophorose (in the case of a 1:1 ratio) increases of about 13%. This parallel effect can probably be included in the reduction of the experimental ρ_{shell} but it cannot justify it completely. A real loss in the water amount must then be taken into account.

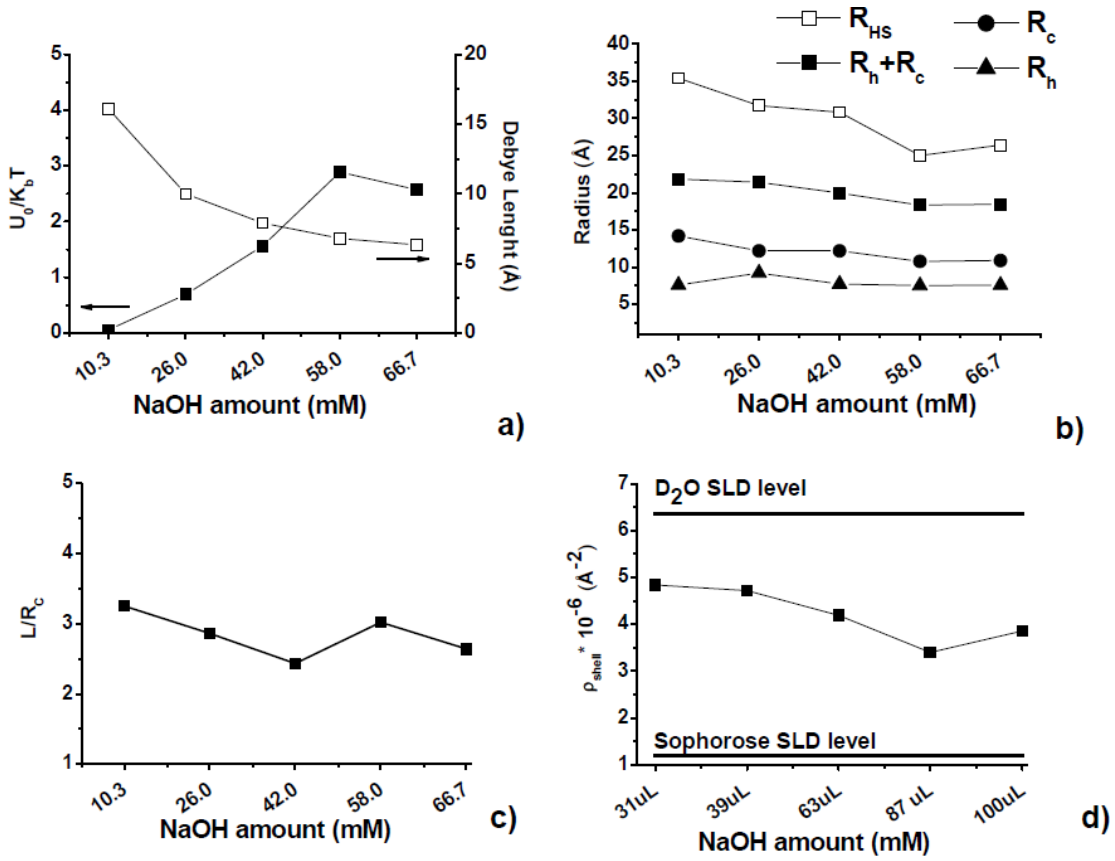

Figure 4 – (a) Evolution of the fitted Yukawa potential strength, U_0/K_bT, and calculated Debye length, as defined, respectively, in Eq.3 and Eq.5. Numerical parameters corresponding to R_h, R_c and hard-sphere radius obtained from the fit are reported in (b). Eccentricity, L/R_c, is given in (c). The Scattering Length Density (SLD), calculated from the α-parameter defined in Eq.1) of the shell, ρ_{shell}, is reported in (d). R_h and R_c refer to, respectively, the size of the hydrophilic head and core radii (see Figure 2).

Base effects. In this section we explore the effect of changing the nature of the base (NaOH, aqueous NH_3, KOH and $Ca(OH)_2$) on equimolar SL-COOH solutions. Figure 5 and Figure 6a-d respectively present the fitted SANS spectra and the corresponding fit parameters. The raw data on Figure 5 show the strong effect of the type of base on the micellar SL-COOH environment. Whereas in presence of NaOH (66.7 mM) and KOH the curves appear very similar, showing the strong repulsive intermicellar interactions also in presence of KOH, the effect of an excess of aqueous ammonia (black circles) is much milder and very similar to NaOH at 10.3 mM, reported on the same figure for comparison purposes. On the contrary, the effect of $Ca(OH)_2$ is definitely much more important on the intermicellar interactions and in particular one can observe: 1) the loss of the interaction peak, typical in KOH and NaOH

systems; 2) the lower intensity of the plateau in the mid-q range below 0.07 $Å^{-1}$. These systems have been fitted using the same form and structure factors as used for NaOH. Please note that the concentration value for $Ca(OH)_2$, 66.7 mM, refers to the final $[OH^-]$, whereas $[Ca^{2+}]$= 33.3 mM.

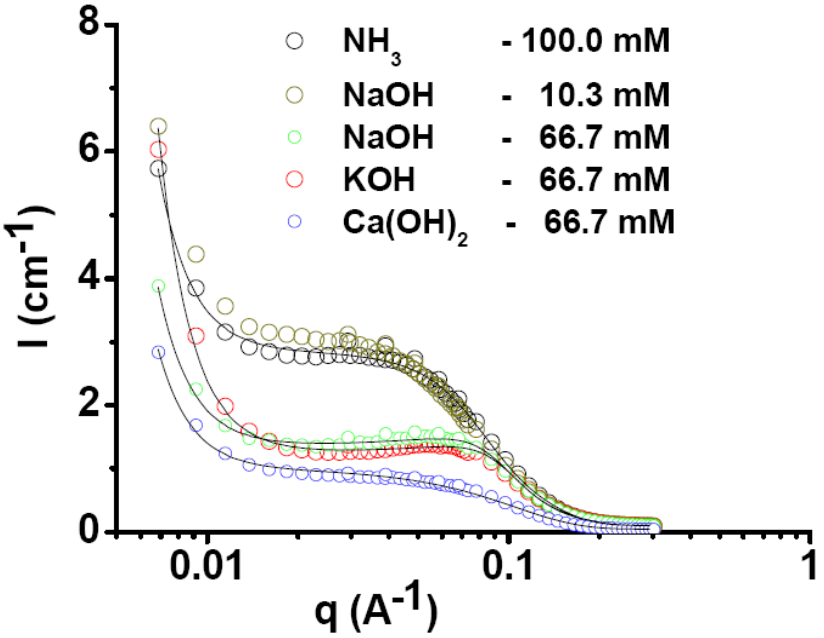

Figure 5 - SANS spectra recorded on a SL-COOH system to which the nature of the added base is varied. The values indicate the base concentration. Solid lines represent the fits obtained using an ellipsoid form factor and a Yukawa interaction potential. The concentration value for $Ca(OH)_2$, 66.7 mM, refers to the final $[OH^-]$, whereas $[Ca^{2+}]$= 33.3 mM

The evolution of U_0/K_bT is given in Figure 6a. As commented before, the positive values obtained for all cations in the fit is the typical sign of repulsive intermicellar interactions, indicating that the process of installing negative charges at the micellar surface is not base-dependent. Nevertheless, the absolute value is different when passing from NH_3 to $Ca(OH)_2$. When aqueous ammonia is used, the interaction is mild and the U_0/K_bT is comparable to the ones observed for low NaOH concentrations (Figure 4a): U_0/K_bT= 0.5 for NH_3 to be compared to U_0/K_bT= 0.1 and 0.7 for, respectively, NaOH at 10.3 mM and 26.0 mM. This is also true for R_{HS}, whose value (32.2 Å) for NH_3 is contained in the 31-35 Å interval measured for NaOH at 10.3 mM and 26.0 mM (Figure 4b). Upon addition of KOH, NaOH (at 66.7 mM) and $Ca(OH)_2$, U_0/K_bT undergoes a 5-fold increase, a clear sign of stronger repulsive interactions. In terms of the typical micellar radii, R_c is always below 15 Å, which still suggests a possible bending of the oleic acid moiety. In addition, both the total radius, R_c+R_h, and R_{HS} (Figure 6b), decrease when going from NH_3 to $Ca(OH)_2$.

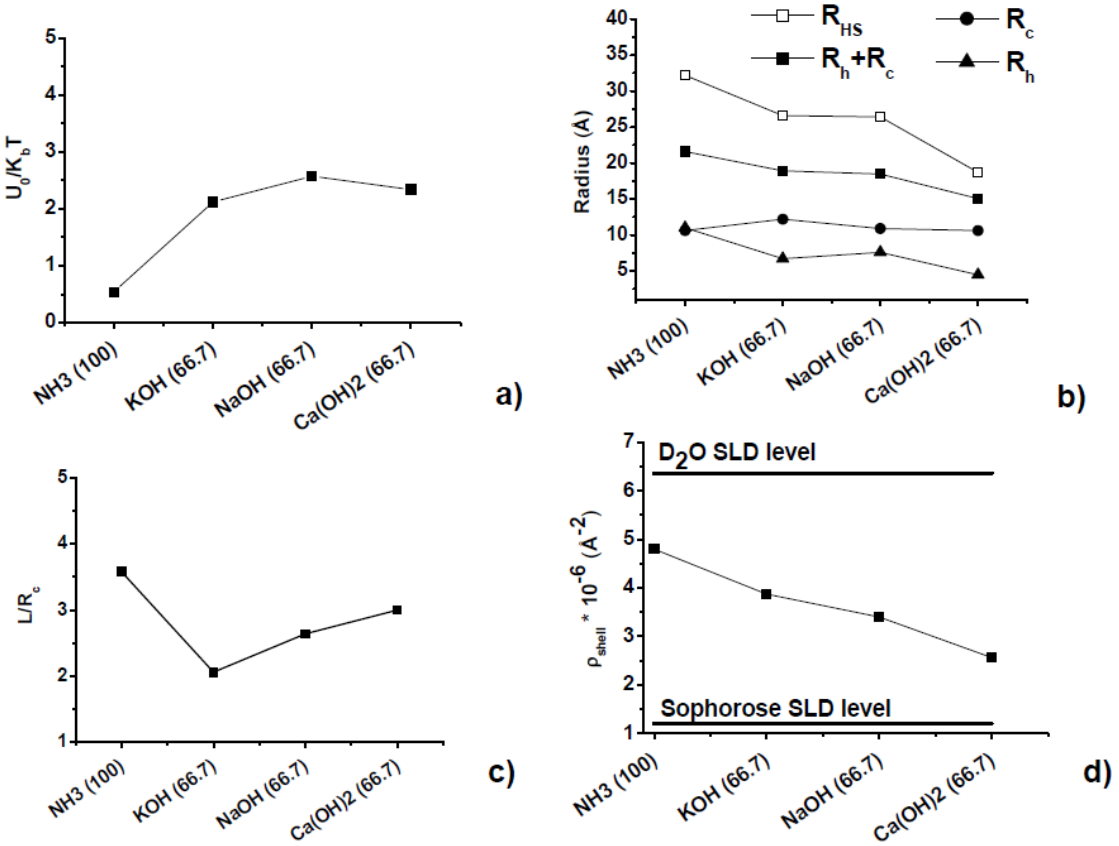

Figure 6 – Evolution of the numerical parameters corresponding to the fits performed on the systems described in Figure 5. Concentration values in brackets are in mmol units. U_0/K_bT is given in (a). R_{HS}, R_h, R_c and R_h+R_c are reported in (b). The eccentricity, L/R_c, is given in (c) while the Scattering Length Density (SLD, calculated from the α-parameter defined in Eq.1) variation is reported in (d). R_h and R_c refer to, respectively, to the hydrophilic head and core radii. Numerical fit values given for the $Ca(OH)_2$ system are those obtained for Fit 2 in Figure 7. For the meaning of $Ca(OH)_2$ concentration, please refer to Figure 5.

For aqueous ammonia, we tested two concentrations, 50 mM (not shown) and 100 mM (Figure 5). Despite the excess concentration used in this study (100 mM), this base provides the smallest impact on the SL-COOH intermicellar interactions. Aqueous ammonia is a weak base and the corresponding ionization degree of SL-COOH is smaller with respect to all other systems. In fact, the measured pH of the $[NH_3]$= 100 mM is about 4.9, which is actually comparable to the pH of the 10-fold less concentrated NaOH system at 10.3 mM (pH= 4.6). In Figure 5, SANS spectra of NH_3 (100 mM) and NaOH (10.3 mM) are almost superimposable and the corresponding fit values are close. When KOH and NaOH are used at 66.7 mM, the composition of the micellar surface changes. First of all, U_0/K_bT falls in the 2.5 range and, secondly, SLD also decreases in the range $3.5–4 \cdot 10^{-6}$ $Å^{-2}$, indicating an undergoing dehydration process in the sophorose layer. Micellar radii (R_c and R_h) and R_{HS} are comparable for these systems while ellipticity (L/R_c) seems to be slightly higher for the Na^+ system. These features may be expected for these two cations which have a comparable binding activity.

The effect of $Ca(OH)_2$, whose concentration was chosen so to provide an equimolar, final, amount of OH^- groups with respect to the other base systems, deserves a specific discussion. As shown in Figure 5, the spectrum of SL-COOH in the presence of $Ca(OH)_2$ is remarkably different. In particular, the interaction hump disappears in favour of a plateau of lower intensity at $q < 0.1$ Å^{-1}. To explain this behaviour, we raise some possible explanations. Even if the nominal volume fraction of SL-COOH in solution is the same for all systems, one can image a disruptive effect of Ca^{2+} on the micelles, thus reducing the number of scattering objects with a consequent loss in the spectrum intensity.

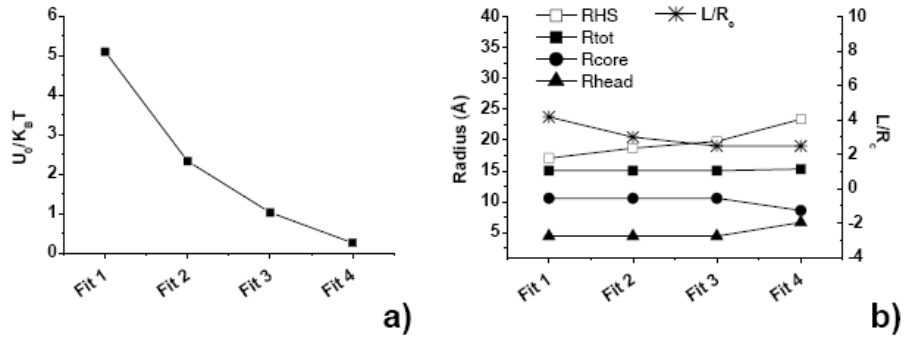

Figure 7 – Fit-dependent evolution of the (a) Yukawa potential, U_0/K_bT, (b) micellar radii and eccentricity L/R_c for the $Ca(OH)_2$ system. All other fit parameter are kept constant.

Another possible explanation deals with considering a combination of strong repulsive interactions with related elongation of the micelle. The according variation of the main fit parameters is reported in Figure 7, where the results of several test fits performed on the $Ca(OH)_2$ curve in Figure 5 are reported. For large (strong repulsive interactions) U_0/K_bT values (Fit 1 and Fit 2 in Figure 7a), one finds small R_{HS} (empty squares in Figure 7b) and large L/R_c (stars in Figure 7b).

Finally, the third explanation considers strong ion binding of Ca^{2+} to the micellar surface, thus screening the effective negative charges. This case is well-known for ionic surfactants for which the interaction peak disappears at high ionic strength.[25] This scenario is nicely described by Fit 3 and Fit 4 (Figure 7), which are characterized by smaller (weak repulsive interactions, that is small effective charge) U_0/K_bT values and consequent small L/R_c (< 2.5) ratios, rather suggesting the existence of non-interacting spherical micelles. In all cases, the Debye length is kept constant in the fits and no practical influence was found on the core radius (R_c) and sophorose layer (R_h) levels.

The first hypothesis is unlikely to be correct, as there is no apparent reason for Ca^{2+} to act as a micellar disruptor. The second hypothesis is highly probable but in this case the results of the fit show a large difference between R_{HS} (~18 Å) and the ellipsoid largest dimension L (~44 Å,

calculated from R_c and L/R_c for Fit 1), which raises questions on the validity of the fitting model, because one expects L to be smaller or comparable to R_{HS}. The third hypothesis is also highly probable but that would not explain the reason behind the intensity loss at $0.01 < q$ ($Å^{-1}$) < 0.1. Finally, both hypothesis 2 and 3 raise the question about the eccentricity (L/R_c) trend, as one expects elongation of the micelles for small U_0/K_bT, which is not the case neither in Fit1 nor in Fit4. Even if more probing experiments would be necessary, several arguments discussed below support a combined scenario, for which the strong repulsive interaction potential expected at the concentration of $Ca(OH)_2$ used here is screened by the strong adsorption of Ca^{2+} ions on the slightly eccentric micelles. Fit 2 reported in Figure 6 expresses a good compromise between the second and third hypothesis.

First of all, the same system at slightly higher $Ca(OH)_2$ amounts (result not shown) is best fitted using fairly large eccentricities ($L/R_c \sim 3$) but small U_0/K_bT values (~ 3). Any fit attempt using a spherical particle model requires the use of very large values of polydispersity (> 0.5), which would be an unreal solution. This seems to be coherent with the second hypothesis if interactions are screened by the strong adsorption of the Ca^{2+} cation, which would have an effect on the effective Debye Length, λ. Even if this parameter was kept constant for all fits, we show in the simulations given in Figure 8 its paramount importance in connection with U_0/K_bT and L/R_c.

For a model system (relevant numerical parameters of the simulation are given in the legend of Figure 8), the effect of U_0/K_bT is shown in Figure 8a. For a large λ value (20 Å) and small eccntricity ($L/R_c= 2.5$), the interaction peak disappears at $U_0/K_bT< 3$. Low U_0/K_bT values do not affect much the plateau intensity, as demonstrated by the dotted curves.

This plateau height is actually more affected by the eccentricity (Figure 8b): at high L/R_c, the interaction peak disappears in favour of a plateau and the corresponding intensity is reduced to about $I= 1.6$ cm^{-1} whereas $I> 3$ cm^{-1} in the reference spectrum (dotted line). Finally, the effect of Debye Length on the interaction peak is shown in Figure 8c. For average values of U_0/K_bT (5) and L/R_c (2.5), which can be realistic for $SL\text{-}COO^-/Ca^{2+}$, the plateau is obtained for λ values below 5 Å, which is also realistic at the typical Ca^{2+} concentrations used in this study.

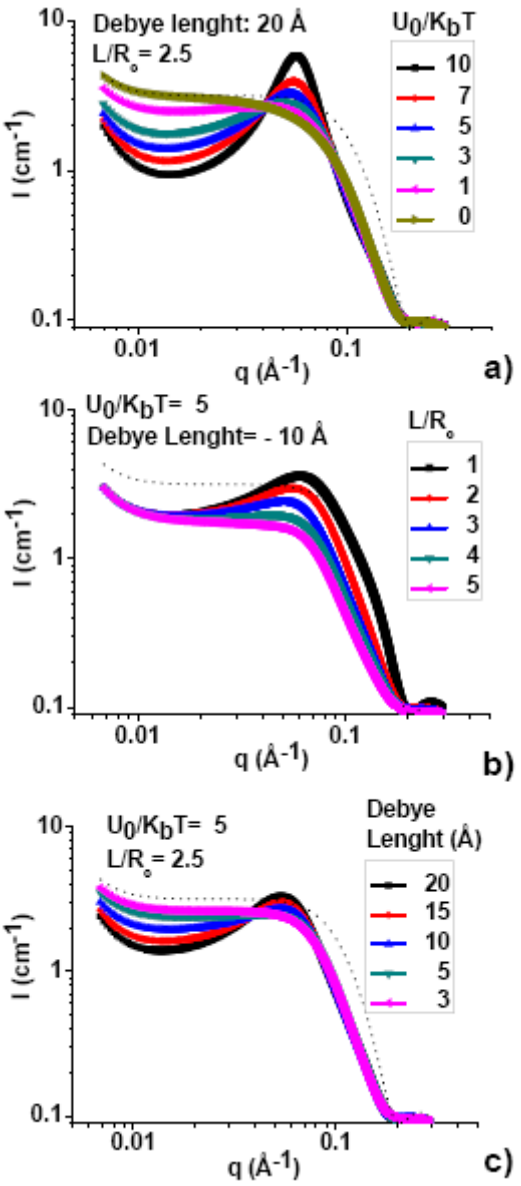

Figure 8 - Influence of (a) U_0/K_bT, (b) L/R_c and (c) Debye Length on simulated I(q) spectra. The most important imposed parameters are given on top of each series of simulation. All other parameters are the same for all simulations: Rc= 15 Å, Rc= 8 Å, α= 0.7, ϕ= 0.05, R_{HS}= 30, I_0= 4.5. The dotted curve represents the same systems composed of monodispersed spherical micelles (L/R_c= 1) with no interactions (U_0/K_bT= 0).

In the absence of a clear-cut answer obtained from the fit, the simulation above indicates that the classical effect of strong repulsive interactions (= the scattering peak) can be masked by a combination of short Debye lengths and micellar elongation, which can also contribute to reduce the effective spectral plateau intensity. This discussion seems to support the hypothesis according to which, despite an expected repulsive interaction comparable to the one observed for monovalent cations, strong binding of Ca^{2+} to the COO^- groups screens the electrostatic interactions thus inducing the formation of longer micelles. For this phenomenon to occur, an effective Debye length is required instead of the theoretical one calculated in Eq.5. Is this

reasonable? To evaluate this point, we will discuss hereafter the binding behaviour of the cations tested in this study and in particular of Ca^{2+}.

The binding affinity of Ca^{2+} (with respect to K^+ and Na^+) to carboxylates should be analyzed in relationship to the well-known Hofmeister Series[26] (HS). HS refers to the variation of solubility (salting in/out) of proteins in water caused by the presence of ions and it has been used to describe the counterion effect on the micellization behaviour of surfactants (CMC, ion binding affinity, solvation, aggregation number, lower critical micellization temperature, etc). As a general rule, strongly hydrated counterions (kosmotropes) are less tightly bound to the charged micellar surface, as they disturb the hydration of the surfactant, while poorly hydrated counterions (chaotropes) improve water structuring around the surfactants, thus promoting stronger ion binding to the micellar surface. Generally, by looking at the hydrated ionic radius, predictability of the counterion/micelle binding affinity is possible. The theoretical order expected from weak to high binding affinity is $Mg^{2+} > Ca^{2+} > Sr^{2+} > Ba^{2+} > Li^+ > Na^+ > K^+ > Rb^+ > Cs^+$, where Mg^{2+} has the lowest binding affinity. In reality, the effective binding affinity, and related macroscopic physico-chemical properties of the counterion/micelle couple, can significantly vary from this order, depending on many variables like the type of amphiphiles, its headgroup, [27,28] solvent,[29] temperature, pH, ionic strength, concentration of the amphiphiles. For instance, the binding affinity of Mg^{2+} for the anionic dodecylsulfate surfactant in water at 30°C at low ionic strength is higher than the expected monovalent Na^+ and K^+ cations.[30] For calcium, it was found a reduction in micellar radii due to strong Ca^{2+} binding to casein micelles in their colloidal stability range. Interestingly, it was found that Ca^{2+} can induce the elongation of surfactin biosurfactant micelles,[31] testifying the strong mutual interactions, which were also reported in presence of carboxylates in the palmitic acid fatty acid.[32] In our specific case, in comparison to these studies, we make the hypothesis that the deprotonated SL-COOH micellar system experiences a strong Ca^{2+} binding. In this case, the water content is expected to be reduced at the micellar outer interface, as actually found in all our fits and as represented in Figure 6d for Fit 2. This occurs despite the fact that Ca^{2+} is a typical hydrophilic ion. One should then imagine that the coordination sphere of Ca^{2+} is replaced by equivalent hydrophilic interactions which are competitive with those generally occurring with water. This is not surprising if one considers the actual environment at the micellar surface and which is mainly constituted by carboxylates (from COO^-) and hydroxyl groups (OH) from sophorose. This can be regarded to as a typical case in which an ionic and a non-ionic group characterize the micellar surface at the same time. Even if it was shown long ago[33] that in similar cases the electrostatic interaction between the ionic surfactant and the

counterion drive its binding, it was also assumed that possible secondary counterion/non-ionic interactions may contribute to perturbate the system, as reported in a carboxylic acid containing pluronic-related surfactant.[34] Additional data recorded on proteins also confirm the crucial role that carboxylate groups play on the binding of hydrophilic divalent cations with respect to monovalent ones.[35] If we compare literature data with ours, we could propose the hypothesis according to which the K^+, Na^+, Ca^{2+} cation series binds stronger to the external surface of the deprotonated SL-COOH ellipsoidal micelles, in which the sophorolipid aliphatic chain is most likely bent outward. If the interaction with calcium is too strong, then one can expect to measure a lower effective micellar charge, which is screened by calcium itself, as typically found for cationic surfactants in the presence of large amounts of salt.[25] Interestingly enough, it is known that screening parameters κ differing from the theoretical values (Eq.5) predicted by the Gouy-Chapman Debye-Huckel Poisson-Boltzmann theory can be recorded for cations interacting with phospholipids.[36,37] This was observed for Na^+-based systems[36] and, in particular, for Ca^{2+}-based solution, which have particularly been addressed of being non-ideal.[37] In this study, κ was calculated using Eq.5 and kept constant to reduce the number of free variables in the fit but, given its effect on the fit based on the simulations in Figure 8c, it is highly possible that the effective Debye lengths for the SL-COO^-/Ca^{2+} strongly differ from the theory.

As a last remark, possible variation of the theoretical volume fraction, ϕ, can also be considered. This parameter was fixed in the fitting process performed in this work because the sophorolipid concentration is the same throughout the study. In reality, one could imagine the existence of an effective ϕ that can slightly vary from one system to another. All SANS spectra shown in this study present a low-q signal typical of large assemblies governed by long-range attractive interactions. We have already shown that in Regime 3[15], at low sophorolipid concentration and excess of base, most small micelles are probably disrupted in favour of larger aggregates, thus showing a clear effect on the effective number of scattering objects. Even if this aspect was not studied further, one should be aware that the strong signal at $q< 0.01$ $Å^{-1}$ detected on all systems in Figure 3 and Figure 5 may hide an uncertain amount of matter under the form of large aggregates and that does not contribute to the SANS intensity in the mid-q region above 0.01 $Å^{-1}$. Evaluation and quantification of the large scale aggregates is very difficult because their nature and amount seems to vary with time at a given concentration, as shown in the next section.

Time effects. In a previous study[8] it was reported that time strongly affects the assembly of sophorolipids in aqueous solutions. In the following section we report a series of SANS experiments that investigate the effect of time (from 8 to 36 days) on the nanometer-scale assembling of SL-COOH. As shown in Figure 9a for regime 2, all spectra up to 21 days are very close and are typical of repulsive intermicellar interactions, as abundantly discussed above. The fits and corresponding value evolution are presented in Figure 9b. In terms of L/R_c, an average value of 2.4 is obtained and no specific evolution over time can be put in evidence; as for the SLD, indicating the water content in the micellar shell, the same observation apply as no specific evolution can be analyzed. On the contrary, U_0/K_bT and R_{HS} do present a significant evolution with time: the first one constantly increases, thus indicating the evolution of the system towards more repulsive intermicellar interactions; the hard-sphere radius also becomes smaller with time. Such a relatively strong time-dependency seems to confirm the previously published results, even if the scales of investigation are not fully comparable (nanometer, here, and micrometer in Ref.8). For sake of comparison, we have also checked the effect of time on regime 1 and 3, where either isolated micelles are formed (regime 1) or disruptive effects occur in favour of large-scale tubular aggregates (regime 3).[15] The time effects SANS results for Regime 1 and 3 are shown, respectively, in Figure 9c and d. For Regime 1, all spectra up to 21 days are actually very similar, which is not the case for Regime 3. After 36 days (blue stars) and for all regimes, all spectra show a systematic difference with respect to those acquired at previous time-delays. This qualitative description indicates that, if compared to regime 3 where the spectral differences indicate lack of stability of the micellar aggregates over 36 days, time seems to have a rather limited, mildly detectable, effect on both regimes 1 and 2.

At the end of the previous section we advanced the idea that the loss in intensity of the experienced in the Ca^{2+} system could also be due to the formation of large aggregates (enhanced scattering at $q< 0.01$ Å) instead of the expected nanoscale micelles scattering in the mid-q region. This effect is rather clear in the time-dependent experiments performed in regime 3. In this case, the fitted intensity, I_0, for the experiments shown in Figure 9d are 0.21, 0.12, 0.14 and 0.00, showing the unpredictable effect of micellar shape evolution with time. The actual time-averaged value, 0.12, is about 30 to 40 times smaller than the corresponding time-averaged I_0 measured in regimes 1 and 2, whereas there is only and 10-fold difference in the volume fractions between regime 3 and both regimes 1 and 2. Again, this supports the previously-reported hypothesis that at high pH most micelles are disrupted in favour of larger objects, which will be discussed in more detail later.

Scattering at low-angle ($q < 0.01$ Å^{-1}) can also be qualitatively commented here. This region indicates the presence of attractive interactions between large-scale objects. Even if this was not specifically pointed out before, regime 2 shows a well-defined intensity increase at $q < 0.01$ Å^{-1}. This seems to be always the case, both in fresh solutions (Figure 3) and in aged ones (Figure 9). Due to the lack of specific experiments at $q < 10^{-3}$ Å^{-1} and to a well-defined signal at $0.01 < q < 0.1$ Å^{-1}, this phenomenon could only be clearly stated for regime 3, where a very low signal in the mid-q region drives the attention to the peculiar sophorolipid behaviour at very low-q.[15] Figure 9a shows that low-q scattering is actually present in all regimes. This is quite obvious for regime 2 and 3 while it is less evident for regime 1. Analysis of the slopes can bring precious pieces of information on the nature of the objects but in this study the explored q-scale is not small enough. Preliminary analysis seems to indicate that typical slope values (log-log) between –1 and –2 are measured for regime 2, which are typical values for, respectively, tubules (-1) and vesicles (-2) larger than 500 Å. As a common observation, the slopes seem to vary without a specific trend, which suggests that time does not have a systematic effect towards the growth of larger micellar aggregates.

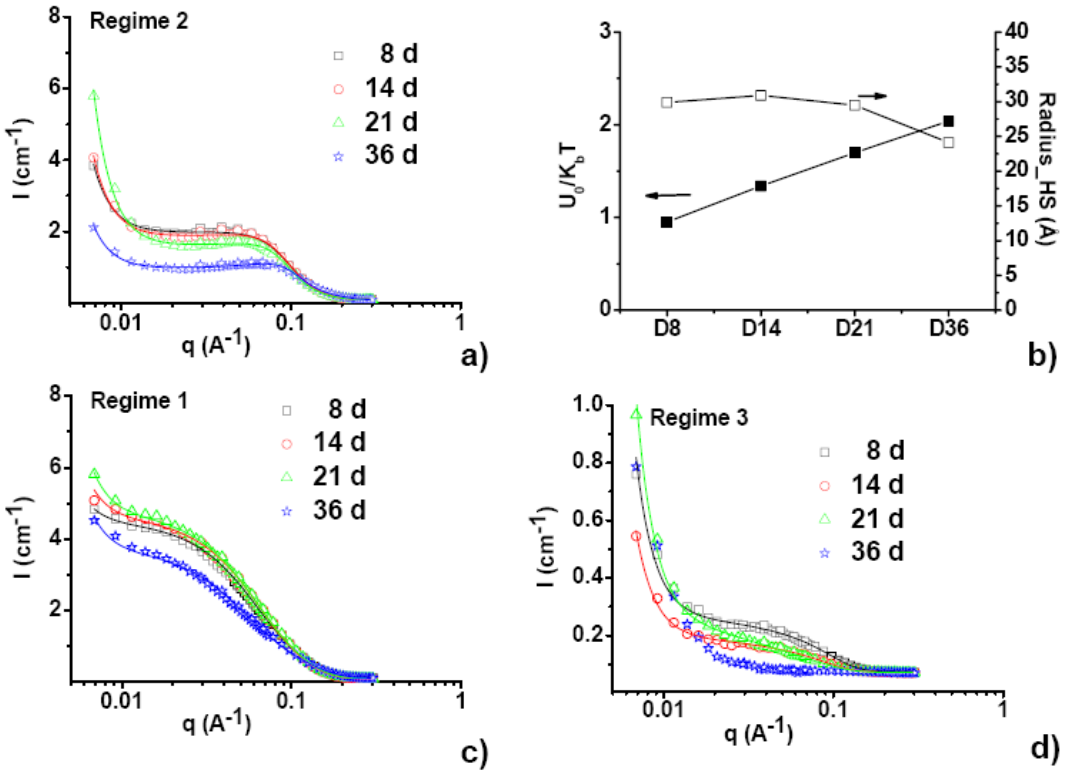

Figure 9 –(a) Time-dependant SANS spectra recorded on a SL-COOH system in regime 2 after 8, 14, 21 and 36 days (D8, D14, D21, D36) from preparation. (b) Time evolution of U_0/K_bT and RHS for regime 2. Time-dependant SANS spectra recorded on regime (c) 1 and (d) 3.

To better clarify the influence of time, we also performed cryo-TEM experiments on regime 2 at the same time delays. Overall, the results confirm the lack of clear trend in the shape evolution of the large-scale aggregates, as suggested by SANS spectra. Nevertheless, it is possible, from a short selection of images shown in Figure 10, to better identify the variety of objects and, to a less extent, make the hypothesis on the way some of them form. On the basis of SANS spectra analysis, Penfold at al.[16] have advanced several hypotheses on the shape of various sophorolipids mixtures but lack of microscopy data could not confirm them. Figure 10a-d gives a good idea of the typical heterogeneity existing in Regime 2 between 8 and 36 days. The section under study is contained in the thin, carbon-free, glassy water layer and each number in the figure is described as follows: 1) the dotted rectangle encloses a zone which is richer in nanoscale micelles undergoing intermicellar interaction, coherently with the SANS analysis. This is confirmed by the corresponding Fourier Transform (FT) showing a scattering ring. 2) The second rectangle is located in a micelle-poor region, whose FT treatment shows a more diffuse signal. 3) In the b and c images (3-labelled arrows) of Figure 10, vesicles of about 18 nm coexist with nanoscale micelles present in the background. 4) Arrow number 4 points at an object which seems to be constituted of three distinct vesicles merging together, where the size of each individual vesicle is between 16 and 18 nm. 5) Large aggregates are abundantly found, as identified by arrows 5 in Figure 10 a and d. These fractal-type aggregates, whose typical sizes (> 20 nm) largely justifies the intense low-q scattering signal in SANS spectra, are regularly observed but at the moment it is unclear how to isolate and stabilize them.

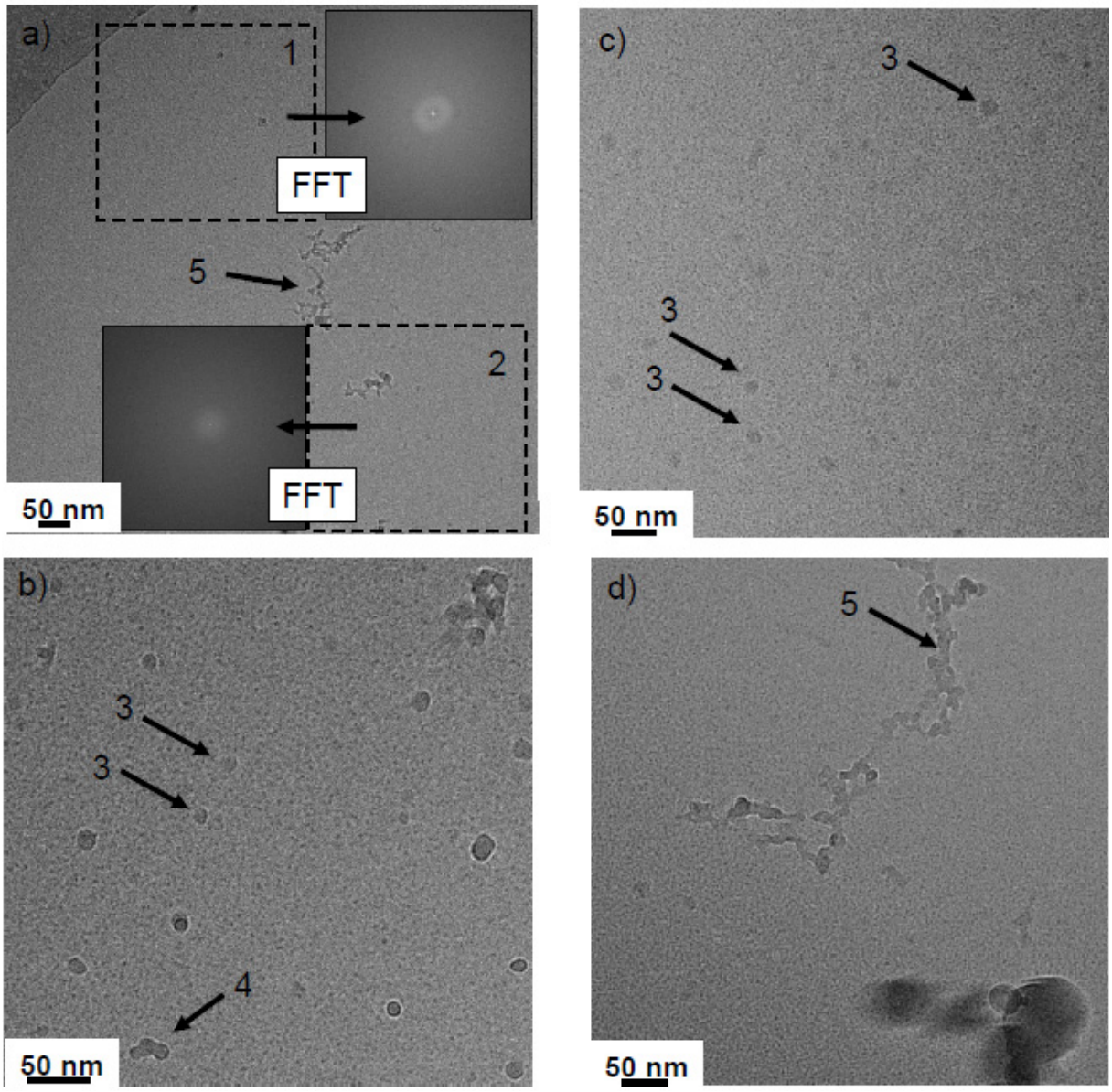

Figure 10 – Cryo-TEM observations done on the SL-COOH sample in regime 2 after (a) 8 and (b, c) 14 and (d) 36 days. (1) Micelles undergoing intermicellar interaction, confirmed by the corresponding Fourier Transform (FT) on the side; (2) micelle-poor region with corresponding FT; (3) single vesicles; (4) vesicles suppositively merging together; (5) large fractal-type aggregates (> 20 nm).

Cryo-TEM is of great help to complement SANS data at very low q-values. First of all, we could observe the formation of large aggregates. Unfortunately, our effort to relate time with growth and size of the aggregates themselves was unfruitful. Despite our systematic study at all evolution times, we could only confirm the lack of systematic growing behaviour for these larger structures. In fact, no specific trend could be found, indicating that a fraction of sophorolipids can always form vesicles, which merge into larger structures to finally form large-scale fractal aggregates. To a certain degree, this conclusion is coherent with the previous observation of Zhou et al.[8], even if here we go much further, demonstrating that the

system can be highly heterogeneous and time has little effect on the micelles, which constitute the majority of the sample in regime 2. If this behaviour remains partly unexplained, several works have been reported in literature where an unpredictable assembling behaviour of specific block copolymers has been described and referred to as "schizophrenic micelles". As reported by Andre et al.,[38] the term 'schizophrenic' denotes the ability of a specific compound (an AB block copolymers in their case) to form a core-shell micelle where the reciprocal chemical composition can be inversed (either A-core or inverse B-core) by varying the pH, and/or the temperature. Effect of temperature is well-known for N-isopropyl-acrylamide (NIPAM) containing block-copolymers, for which the hydrophilic/hydrophobic balance changes if the experimental temperature is below or above the copolymer typical Lower Critical Solution Temperature (LCST). Even if a specific LCST has not been reported for sophorolipids, one can suppose that temperature does have a non-negligible effect on the shape and size of the micelles, thus leading to a heterogeneous medium. Smith et al.[39], for instance, have reported about the "schizophrenic" behaviour of a NIPAM-based block copolymer: as a function of the temperature and pH it can form either micelles or vesicles. This is also the case in the work of Andre,[38] where a combination of small micelles and large-scale objects can be obtained at pH= 12 and 23°C. For sophorolipids, we systematically let the system evolve at room temperature, which may be close enough to a transition point unknown at the moment.

Conclusion

Using a combination of SANS with numerical modelling, we put in clear evidence the micellar surface charge evolution of acidic sophorolipids in water when exposed to increasing millimolar concentrations of different bases. In the first place, we identified that micelles can be described by ellipsoids of revolution with a core-shell interface. Then, using NaOH as only source of pH variation, we could follow the evolution of the interaction repulsive potential (U_0/K_bT, a combination between hard sphere and screened Coulomb potentials) between sophorolipid micelles, which we prove to become more and more negatively charged. The effective charge, Z, can be tuned from about 0.5 to 5.3 when final [NaOH] goes from 10.3 mM to 66.7 mM. A similar behaviour occurs if other bases are used but at a different extent, thus putting in evidence either the role of the pH or the counterion.

In aqueous ammonia, a weak base, at 100 mM the SL-COOH system behaves like in presence of a ten-fold less concentrated NaOH solution at equivalent pH. If this could suggest that pH is the only parameter playing an important role in the control of the SL-COOH intermicellar

interactions, we also show that the nature of the base, that is the counterion, is also equally important. In presence of $Ca(OH)_2$, the strong binding affinity of Ca^{2+} for COO^- drives the system towards a better surface charge screening, which has the effect of reducing the repulsive potential, the effective surface charge and elongating the micellar length. Our data also confirms the previous hypothesis on the local SL-COOH conformation. Upon increasing the pH, the sophorolipid aliphatic chain has a strong tendency to bend outward.

Finally, some insights were given on the shape evolution as a function of time between 8 and 36 days at constant room temperature. SANS experiments actually show that time does not seem to have a large effect neither on isolated nor on interacting micelles but it does have a strong effect on the surface charge. In addition, large-scale objects (d > 50 nm) are the ones affected by this parameter. Cryo-TEM experiments indicate the spurious presence of vesicles (d~ 18 nm) and the possibility that these emerge into larger fractal aggregates. Unfortunately, keeping the samples at room temperature does not provide a good control over such aggregates, thus suggesting that such a parameter, in combination with time itself, needs to be explored further.

Acknowledgements

The research leading to these results has received funding from the European Community's Seventh Framework Programme (FP7/2007-2013) under Grant Agreement n° Biosurfing/289219. Marianne Impéror-Clerc (LPS, Université Paris Sud-11, France) is ahighly acknowledged for helpful discussions.

References

[1] Kjellin, M.; Johansson, I. *Surfactants from Renewable Resources*, John Wiley & Sons, Ltd: West Sussex, 2010
[2] von Rybinski, W.; Hill, K. Alkyl Polyglycosides—Properties and Applications of a new Class of Surfactants *Angew. Chem. Int. Ed*. **1998**, *37*, 1328-1345
[3] Stubenrauch, C. Sugar Surfactants – Aggregation, Interfacial, and Adsorption Phenomena *Curr. Op. Coll. Interf. Sci*. **2001**, *6*, 160-170
[4] Hoffmann, B.; Platz, G. Phase and Aggregation Behaviour of Alkylglycosides *Curr. Op. Coll. Interf. Sci*. **2001**, *6*, 171-177
[5] Rau, U.; Hammen, S.; Heckmann, R.; Wray, V.; Lang, S. Sophorolipids: a Source for Novel Compounds *Ind. Crops Prod*. **2001**, *13*, 85–92
[6] Tulloch, A. P.; Hill, A.; Spencer, J. F. T. Structure and Reactions of Lactonic and Acidic Sophorosides of 17-Hydroxyoctadecanoic Acid *Canad. J. Chem*. **1968**, *46*, 3337-3351
[7] Asmer, H.-J. ; Lang, S.; Wagner, F.; Wray, V. Microbial Production, Structure Elucidation and Bioconversion of Sophorose Lipids. *J. Am. Oil. Chem. Soc.* **1988**, *65*, 1460-1466
[8] Zhou, S.; Xu, C.; Wang, J.; Gao, W.; Akhverdiyeva, R.; Shah, V.; Gross, R. Supramolecular Assemblies of a Naturally Derived Sophorolipid *Langmuir* **2004**, *20*, 7926-7932
[9] Develter, D. W. G.; Fleurackers, S. J. J. *Surfactants from Renewable Resources*, John Wiley & Sons, Ltd: West Sussex, 2010; pp. 213-238
[10] Maingault, M. Use of Sophorolipids and Cosmetic and Dermatological Compositions, WO/1995/034282A

[11] Van Bogaert, I. N. A.; Saerens, K.; De Muynck, C.; Develter, D.; Soetaert, W.; Vandamme, E. J. Microbial Production and Application of Sophorolipids *Appl. Microbiol. Biotechnol.* **2007**, *76*, 23–34

[12] Shete, A. M.; Wadhawa, G.; Banat, I. M.; Chopade, B. A. Mapping of Patents on Bioemulsifier and Biosurfactant: a Review *J. Sci. Ind. Res*. **2006**, *65*, 91-11

[13] Fu, S. L.; Wallner, S. R.; Bowne, W. B.; Hagler, M. D.; Zenilman, M. E.; Gross, R.; Bluth, M. H. Sophorolipids and Their Derivatives are Lethal Against Human Pancreatic Cancer Cells *J. Surg. Res.* **2008**, *148*, 77-82

[14] Baccile, N.; Nassif, N.; Malfatti, L.; Van Bogaert, I. N. A.; Soetaert, W.; Pehau-Arnaudet, G.; Babonneau, F. Sophorolipids: a Yeast-Derived Glycolipid as Greener Structure Directing Agents for Self-Assembled Nanomaterials *Green Chem*. **2010**, *12*, 1564–1567

[15] N. Baccile, F. Babonneau, J. Jestin, G. Pehau-Arnaudet, I. Van Bogaert Unusual, pH-induced, self-assembly of sophorolipid biosurfactants, ACS Nano, 2012, 6, 4763–4776

[16] J. Penfold, M. Chen, R. K. Thomas, C. Dong, T. J. P. Smyth, A. Perfumo, R. Marchant, I. M. Banat, P. Stevenson, A. Parry, I. Tucker, I. Grillo, Langmuir, 2011, 27, 8867-8877

[17] M. Chen, C. Dong, J. Penfold, R. K. Thomas, T. J. P. Smyth, A. Perfumo, R. Marchant, I. M. Banat, P. Stevenson, A. Parry, I. Tucker, R. A. Campbell, Langmuir, 2011, 27, 8854-8866

[18] http://didier.lairez.fr/dokuwiki/doku.php?id=pasinet

[19] J. S. Pedersen, Adv. Coll. Interf. Sci., 1997, 70, 171-210; J. S. Pedersen, Modelling of Small-Angle Scattering Data from Colloids and Polymer Systems in Neutrons, X-Rays and Light, Eds. P. Lindner and Th. Zemb, 2002 Elsevier Science B.V., p. 391

[20] J. J. Lebowitz, J. K. Percus, Phys. Rev., 1966, 144, 251; J. B. Hayter, J. Penfold, Molecular Physics, 1981, 42, 109-118

[21] J. S. Pedersen, Monte Carlo Simulation Techniques Applied in the Analysis of Small-Angle Scattering Data from Colloids and Polymer Systems in Neutrons, X-Rays and Light, Eds. P. Lindner and Th. Zemb, 2002 Elsevier Science B.V., p. 381

[22] M. Masuda, T. Shimizu, Langmuir, 2004, 20, 5969-5977

[23] http://www.ncnr.nist.gov/resources/sldcalc.html

[24] Kaibara, K.; Iwata, E.; Eguchi, Y.; Suzuki, M.; Maeda, H. Dispersion Behavior of Oleic Acid in Aqueous Media: From Micelles to Emulsions *Colloid Polym Sci* **1997**, *275*, 777-783

[25] V. K. Aswal, J. Kohlbrecher, P. S. Goyal, H. Amenitsch, S. Bernstorff, J. Phys.: Condens. Matter, 2006, 18, 11399–11410

[26] S. Glasstone, Text Book of Physical Chemistry, 2nd ed., Macmillian, London, 1960, p. 1254

[27] N. Vlachy, B. Jagoda-Cwiklik, R. Vácha, D. Touraud, P. Jungwirth, W. Kunz, Adv. Coll. Interf. Sci., 2009, 146, 42-47

[28] N Vlachy, M. Drechsler, J.-M. Verbavatz D. Touraud, W. Kunz, J. Coll. Interf. Sci., 2008, 319, 542–548

[29] B. Hessa, N. F. A. van der Vegta, , Proc. Nat. Acad. Sci., 2009, 106, 13296–13300

[30] K. Maiti, D. Mitra, S. Guha, S. P. Moulik, J. Molec. Liq., 2009, 146, 44–51

[31] H.-H. Shen, T.-W. Lin, R. K. Thomas, D. J. F. Taylor, J. Penfold, J. Phys. Chem. B 2011, 115, 4427–4435

[32] C. Y. Tang, Z. Huang, H. C. Allen, J. Phys. Chem. B 2010, 114, 17068–17076

[33] J. F. Rathman, J. F. Scamehorn, J. Phys. Chem., 1984, 88, 5807-5816

[34] J. P. A. Custers, L. J. P. van den Broeke, J. T. F. Keurentjes, Langmuir 2007, 23, 12857-12863

[35] J. Kherb, S. C. Flores, P. S. Cremer, J. Phys. Chem. B 2012, 116, 7389−7397

[36] M. E. Loosey-Millman, R. P. Rand, V. A. Parsegian, Biophys. J., 1982, 40, 221

[37] L. J. Lis, V. A. Parsegian, R. P. Rand, Biochemistry, 1981, 20, 1761-1770

[38] X. Andre, M. Burkhardt, M. Drechsler, P. Lindner, M. Gradzielski, A. H. E. Müller, Polym. Mater. Sci. Eng., 2007, 96, 560

[39] A. E. Smith, X. Xu, S. E. Kirkland-York, D. A. Savin, C. L. McCormick, Macromolecules, 2010, 43, 1210-1217